# Practical embedding for ionic materials: Crystal-adapted pseudopotentials for the MgO crystal

Víctor Luaña, J. M. Recio, A. Martín Pendás, M. A. Blanco, and L. Pueyo
*Departamento de Química Física y Analítica Facultad de Química, Universidad de Oviedo, E-33006-Oviedo, Spain*

Ravindra Pandey
*Department of Physics, Michigan Technological University, Houghton, Michigan 49931*
(Received 20 February 2001; published 22 August 2001)

We present a method of deriving effective core potentials (ECP's) for negative and positive ions. These ECP's are adapted to ionic crystals and can be used as components of an embedding model in most quantum chemistry codes. Cluster-in-the-lattice calculations of several defects and impurity centers in MgO are examined as a test.

DOI: 10.1103/PhysRevB.64.104102 PACS number(s): 61.72.Bb, 61.72.Ji, 31.70.Dk

## I. INTRODUCTION

Winter, Pitzer, and Temple (WPT) introduced in 1987 the idea of using effective core potentials (ECP's) to represent the quantum embedding effects of the crystalline environment in cluster-in-the-lattice calculations of ionic materials.[1,2] In such calculations, a finite set of point charges along with the ECP's is also commonly used. Its role is to mimic, as faithfully as possible, the Madelung field of the crystal. Generally, the embedding ECP technique is intended (a) as a method for the addition to the cluster Hamiltonian of an interaction that physically exists in the crystal, and (b) as a scheme to effectively solve some of the technical problems that plague quantum cluster calculations applied to condensed matter. For example, the ECP's provide a barrier against the unphysical escape ''towards the lattice'' of the cluster electron density and also improve the convergence of the self-consistent-field process in total energy calculations.

The WPT embedding scheme can be immediately used in most current quantum chemistry codes[3–6] as they support assigning of ECP's and point charges to arbitrary positions in the lattice. This is, probably, the best practical advantage of the WPT embedding over other techniques proposed so far.[7–11] One of its most serious difficulties, however, is the unavailability of ECP's for negative anions. This is a consequence of methods traditionally used to derive the ECP's[12–14] that require one or more populated orbitals out of the core for which the pseudopotential is being derived. This means, for instance, that an *all-electron* solution of $F^{2-}$ must be obtained before deriving the pseudopotential for $F^{-}$.

Even with this limitation, the WPT embedding has proved to be a valid technique and it has been used in a number of problems and compounds, including $Cu^{+}$:NaF and $Cu^{+}$:NaCl,[1,2,15] $V^{+2}$:$MgF_2$,[16] $Cr^{3+}$:$Al_2O_3$,[17] and $La_2CuO_4$.[18–23]

To alleviate the problem of deriving ECP's for anions, we propose a procedure in this paper that is based on the orbital description of the core being simulated and that does not depend on the existence of any valence set out of this core. This procedure may be viewed as a translation of the *ab initio* model potential (AIMP) formalism of Huzinaga *et al.*[24] to the ECP formalism.

Although free-ion orbital descriptions of positive or negative ions can be used to derive the ECP's, our procedure uses the ionic descriptions self-consistently adapted to the crystal environment provided by the *ab initio* perturbed ion (AIPI) method.[25,26] In particular, the use of the AIPI wave functions solves the problem posed by multinegative ions, which are generally unstable in gas phase and for which empirical recipes such as Watson spheres provide only very crude approximations. From now on, we will use the term ''crystal adapted pseudopotentials'' (CAPS's) to refer to the ECP's derived with the method proposed here.

The rest of the article is organized as follows. The embedding method is presented and analyzed in the next section. Crystal adapted pseudopotentials for the MgO crystal are obtained in Sec. III. In this section we also analyze the cluster-lattice consistency, using results of calculations on pure MgO, and discuss the advantages and difficulties of deficient cluster-lattice partitions. A well-tested cluster model is used in Sec. IV to determine the equilibrium properties of several cationic and anionic MgO defect centers, including both neutral and charged defects. The main conclusions are finally presented in Sec. V.

## II. METHOD

Many local properties of pure and defective solids can be studied with the help of cluster-in-the-lattice calculations. This type of calculation is designed to determine the wave function and energy levels of a system made of a small number of atoms or ions (the *cluster*) embedded into the rest of the crystal (the *lattice*). Since the concept of embedding includes mathematical and physical consistency between the cluster and lattice wave functions, it can properly be described as a case of electronic group separation[9,25] and analyzed in terms of the electronic separability theory (TSE) of McWeeny[27] and Huzinaga.[28]

The cluster ($\mathcal{C}$) is the electron group most interesting for our problem. The lattice ($\mathcal{L}$) is divided into a number of atoms or ions whose representation is known in advance and kept frozen during the cluster calculation. The cluster wave function is obtained by solving the Fock equations corresponding to the effective Hamiltonian

 

$$\hat{\mathcal{H}}^{\mathcal{C}}_{\rm eff}=\hat{\mathcal{H}}^{\mathcal{C}}+\sum_{S\in\mathcal{L}}\sum_{i=1}^{N_{\mathcal{C}}}\{\hat{V}^S_{\rm eff}(i)+\hat{P}^S(i)\}, \tag{1}$$

where $\hat{\mathcal{H}}^{\mathcal{C}}$ is the Hamiltonian of the isolated cluster and $S$ sums over all the ions in the lattice and $i$ over the $N_{\mathcal{C}}$ electrons in $\mathcal{C}$.

The $\hat{V}^S_{\rm eff}(i)$ term represents the potential energy of the $i$th electron in the field due to the frozen group $S$. This effective potential may be expressed as

$$\hat{V}^S_{\rm eff}(i)=-\frac{q_S}{r_{iS}}+\hat{V}^S_{\rm nc}(r_{iS})-\hat{V}^S_x, \tag{2}$$

where $r_{iS}=|\vec{r}_i-\vec{R}_S|$, $q^S$ is the net charge of ion $S$ at $\vec{R}_S$, $\hat{V}^S_{\rm nc}$ corrects the electrostatic potential for deviations from the purely point-charge description, and $\hat{V}^S_x$ accounts for the nonlocal exchange interaction.

When $\hat{P}^S(i)$ in Eq. (1) is chosen as

$$\hat{P}^S(i)=\sum_{k\lambda\in S}|\phi^S_{k\lambda}\rangle(-2\epsilon^S_{k\lambda})\langle\phi^S_{k\lambda}|, \tag{3}$$

this projection operator procures the cluster-lattice orthogonality and corrects the energies for residual nonorthogonalities.[29] In this equation $|\phi^S_{k\lambda}\rangle$ is an occupied orbital with orbital energy $\epsilon^S_{k\lambda}$. This flavor of the TSE equations has been shown[29] to be equivalent to a particular localizing potential in the Adams,[30,31] Gilbert,[32] and Kunz[33] localizing potential formalism.

### A. Embedding in the AIPI method

To proceed further we will introduce some approximations that will lead us to use a lattice description derived from calculations on the host. First, the orbitals of a given lattice center are described as linear combinations of Slater-type orbitals (STO's) centered in the nucleus of that atom or ion:

$$\phi^S_{k\lambda\mu}(\vec{r})=Y_{\lambda\mu}(\theta,\varphi)\sum_a C^S_{k\lambda a}\chi^S_{a\lambda}(r), \tag{4}$$

where the coordinates $(r,\theta,\varphi)$ refer to the $S$ nucleus center, and $\chi^S_{a\lambda}$ is a normalized STO:

$$\chi_{a\lambda}=\mathcal{N}_{a\lambda}r^{n_{a\lambda}-1}e^{-\zeta_{a\lambda}r},\quad \mathcal{N}_{a\lambda}=\frac{(2\zeta_{a\lambda})^{n_{a\lambda}+1/2}}{\sqrt{(2n_{a\lambda})!}}. \tag{5}$$

The superscript $S$, which refers to the ion center, will be omitted except when some confusion could appear.

From Eq. (4) it can be seen that the radial part of the orbital is assumed to be identical for all subspecies with the same principal and angular quantum numbers. This is equivalent to forcing the ions to maintain the $O_3^+$ symmetry characteristic of the free species. This approximation is appropriate for highly ionic materials, which are the main purposed targets of the present method, and it will allow us to derive the CAPS in the usual ECP format.

Given the radial symmetry assumed for the local ionic wave functions, the nonclassical component of the Coulombic radial potential can be exactly written as

$$\hat{V}_{\rm nc}(r)=\sum_\lambda\sum_{a\geqslant b}\rho_{\lambda ab}\sum_{J=-1}^{n_{ab}-2}\omega^J_{\lambda ab}r^Je^{-\zeta_{ab}r}, \tag{6}$$

with

$$\omega^J_{\lambda ab}=-\frac{n_{ab}!}{(J+1)!\,\zeta_{ab}^{n_{ab}-J}}\left(1-\frac{J+1}{n_{ab}}\right) \tag{7}$$

for $J\geqslant -1$, and

$$\rho_{\lambda ab}=(2-\delta_{ab})\mathcal{N}_{a\lambda}\mathcal{N}_{b\lambda}\sum_{k\in\lambda}e_{k\lambda}C_{k\lambda a}C_{k\lambda b}, \tag{8}$$

where $e_{k\lambda}$ is the electronic population of the $k\lambda$ shell, $n_{ab}=n_{\lambda a}+n_{\lambda b}$, and $\zeta_{ab}=\zeta_{\lambda a}+\zeta_{\lambda b}$. The symmetry $\lambda ab\leftrightarrow\lambda ba$ has been used to reduce the sums in Eq. (6).

The exchange operator, on the other hand, is conveniently written as the nondiagonal truncated spectral resolution[24]

$$\hat{V}^S_x=\sum_\lambda\sum_{\mu=-\lambda}^{\lambda}\sum_{a,b}|a\lambda\mu,S\rangle A(\lambda ab,S)\langle b\lambda\mu,S|, \tag{9}$$

where the sum runs over the basis functions of $S$:

$$|a\lambda\mu,S\rangle=\chi^S_{a\lambda}(r)Y_{\lambda\mu}(\theta,\varphi). \tag{10}$$

The elements $A(\lambda ab,S)$ are obtained from the overlap (**S**) and exchange (**K**) one-center matrices according to

$$\mathbf{A}=\mathbf{S}^{-1}\mathbf{K}\mathbf{S}^{-1}. \tag{11}$$

The above spectral resolution, introduced in the context of environment representation by Huzinaga and collaborators,[24] would be exact if a complete multicenter basis set were used to represent the local wave functions of each center. This would require computing multicenter exchange integrals that would dramatically complicate the calculations, and would prevent us from producing the CAPS's in the usual ECP form. The errors introduced in the exchange interactions are diminished by the use of large and diffuse, although monocentric, basis sets for each ion, as it is regularly done in the AIPI calculations. Martín Pendás *et al.*[34] have discussed this topic in length.

It is useful to notice that the projection operator can be written in the form used above for the exchange, namely,

$$\hat{P}^S=\sum_\lambda\sum_{\mu=-\lambda}^{\lambda}\sum_{ab}|a\lambda\mu,S\rangle P(\lambda ab,S)\langle b\lambda\mu,S|, \tag{12}$$

with the **P** matrix elements being defined as

$$P(\lambda ab,S)=\sum_{k\in\lambda}C^S_{k\lambda a}(-2\epsilon_{k\lambda})C^S_{k\lambda b}, \tag{13}$$

where $k$ runs over the occupied orbitals of angular quantum number $\lambda$ and $P(\lambda ab,S)$ is invariant to the change

$\lambda ab \leftrightarrow \lambda ba$. Exchange and projection terms can then be given an equivalent treatment in the analysis and development of the CAPS.

### B. Definition of the crystal adapted pseudopotentials

The target effective core potential form, as it is accepted in most popular quantum chemical codes,[3–6,35] responds to the following expression:[36]

$$\hat{U} = -\frac{q}{r} + \mathcal{U}_L(r) + \sum_{\lambda=0}^{L-1} \sum_{\mu=-\lambda}^{\lambda} |Y_{\lambda\mu}\rangle \mathcal{U}_{\lambda-L}(r) \langle Y_{\lambda\mu}|, \tag{14}$$

$$\mathcal{U}_{\lambda-L}(r) = \mathcal{U}_\lambda(r) - \mathcal{U}_L(r), \tag{15}$$

where $q$ is the nominal charge of the lattice ion, and the spherical harmonics and radial functions are centered at the site of the atomic nucleus. The $\mathcal{U}_L(r)$ and $\mathcal{U}_{\lambda-L}(r)$ radial functions are expressed as linear combinations of Gaussian-type functions (GTF's):

$$\mathcal{U}_l(r) = \sum_{i=1}^{N} B_i^l r^{n_i^l} \exp(-\alpha_i^l r^2). \tag{16}$$

This form has to be compared with the AIPI embedding potential. After some manipulation of the equations in the preceding subsection we can write

$$\hat{V}_{\mathrm{AIPI}} = -\frac{q}{r} + \hat{V}_{\mathrm{nc}}(r) + \sum_{\lambda=0}^{l_{\max}} \sum_{\mu=-\lambda}^{\lambda} |Y_{\lambda\mu}\rangle f_\lambda \langle Y_{\lambda\mu}|, \tag{17}$$

$$f_\lambda = \sum_{a,b} \{\chi_{a\lambda}(r)[-A(\lambda ab) + P(\lambda ab)]\chi_{b\lambda}(r)\}, \tag{18}$$

where $l_{\max}$ is the maximum angular momentum for which the center has nonzero electronic population (e.g., $l_{\max}=1$ for $O^{2-}$).

A direct comparison between Eqs. (14) and (17) indicates that the CAPS will reproduce the AIPI embedding when

$$L = l_{\max} + 1, \tag{19}$$

$$\mathcal{U}_L(r) = \hat{V}_{\mathrm{nc}}(r), \tag{20}$$

$$\mathcal{U}_{\lambda-L}(r) = \sum_{a,b\in\lambda} \chi_{a\lambda}(r)[-A(\lambda ab) + P(\lambda ab)]\chi_{b\lambda}(r). \tag{21}$$

According to Eq. (20), $\mathcal{U}_L(r)$ represents the deviation of the electrostatic lattice interaction with respect to a purely point-charge lattice potential. At very short distances $\mathcal{U}_L(r)$ behaves as

$$\lim_{r\to 0}[-q + r\mathcal{U}_L(r)] = -Z, \tag{22}$$

showing that the electrons in the neighborhood tend to see the attraction of the bare nucleus when they are near enough. For very large distances, on the other hand,

$$\lim_{r\to\infty}[-q + r\mathcal{U}_L(r)] = -q. \tag{23}$$

For $0<r<\infty$, $\mathcal{U}_L(r)$ is negative, thus being an attracting potential. Furthermore, it must be noticed that $\mathcal{U}_L(r)$ works not only on the electrons but on the nuclei too, by modifying the Madelung field of the crystal.

The $\mathcal{U}_{\lambda-L}(r)$ potential acts only on the electrons. It contains the exchange attraction and the core projection repulsion. Its net effect depends on the angular momentum and the nature of the ion but at short distances the Pauli repulsion must always be the dominant effect.

Notice that the equations given above yield the required pseudopotential in numerical form knowing only the core orbitals of the center. At this point, we want to emphasize the two advantages of using the lattice orbitals given by the AIPI crystal calculations instead of free-ion orbitals. First, the AIPI wave functions are self-consistently adapted to the global crystalline environment. Second, many important anions, such as $O^{2-}$ and $N^{3-}$, are stable only within the crystal.

Once the $\mathcal{U}_l(r)$ functions have been numerically evaluated for a given grid, we can find the linear combination of GTF's [Eq. (16)] that best fits the numerical values. To do so we define the weighted square error as

$$\chi^2 = \sum_{k=1}^{K} \left[\frac{\mathcal{U}_l(r_k) - \mathcal{W}_l(r_k)}{\sigma_k}\right]^2, \tag{24}$$

where

$$\mathcal{W}_l(r) = \sum_{i=1}^{N} B_i^l r^{n_i^l} e^{-\alpha_i^l r^2}. \tag{25}$$

The linear, $B_i^l$, and exponential, $\alpha_i^l$, parameters are obtained by minimizing $\chi^2$. The fit is a delicate and nontrivial process if one wants to maintain a reduced number of GTF's in the expansion of the radial functions, $\mathcal{W}_l(r)$. Three aspects of the fitting procedure deserve to be described: (a) the optimization scheme; (b) the fitting grid; and (c) the set of weights, $\{\sigma_k\}$.

With respect to the optimization scheme, two main different strategies have been implemented. In the first technique, the linear coefficients are directly obtained by solving the set of linear equations that result from the minimum condition, $\partial\chi^2/\partial B_i = 0$. The exponential parameters can then be searched by means of a nonlinear optimization using, for instance, the Nelder and Mead simplex or the Fletcher-Powell quadratic methods.[37] It has been found that a geometrical series, $\alpha_j = ab^{j-1}$, can be used as a first step in optimizing the exponential parameters, with the values for $a$ and $b$ easily obtained by minizing $\chi^2$. When two or more exponential parameters become degenerate, the linear equations start to be ill conditioned, and the whole scheme risks being unstable. As an alternative, the Levenberg-Marquardt nonlinear least-squares method[37] can be used to obtain, simultaneously, both the $B_i^l$ and $\alpha_i^l$ parameters.

The grid of radial distances can be chosen using either a linear or a logarithmic series. Care must be taken to make sure that both small and large values or $r$ are well repre-

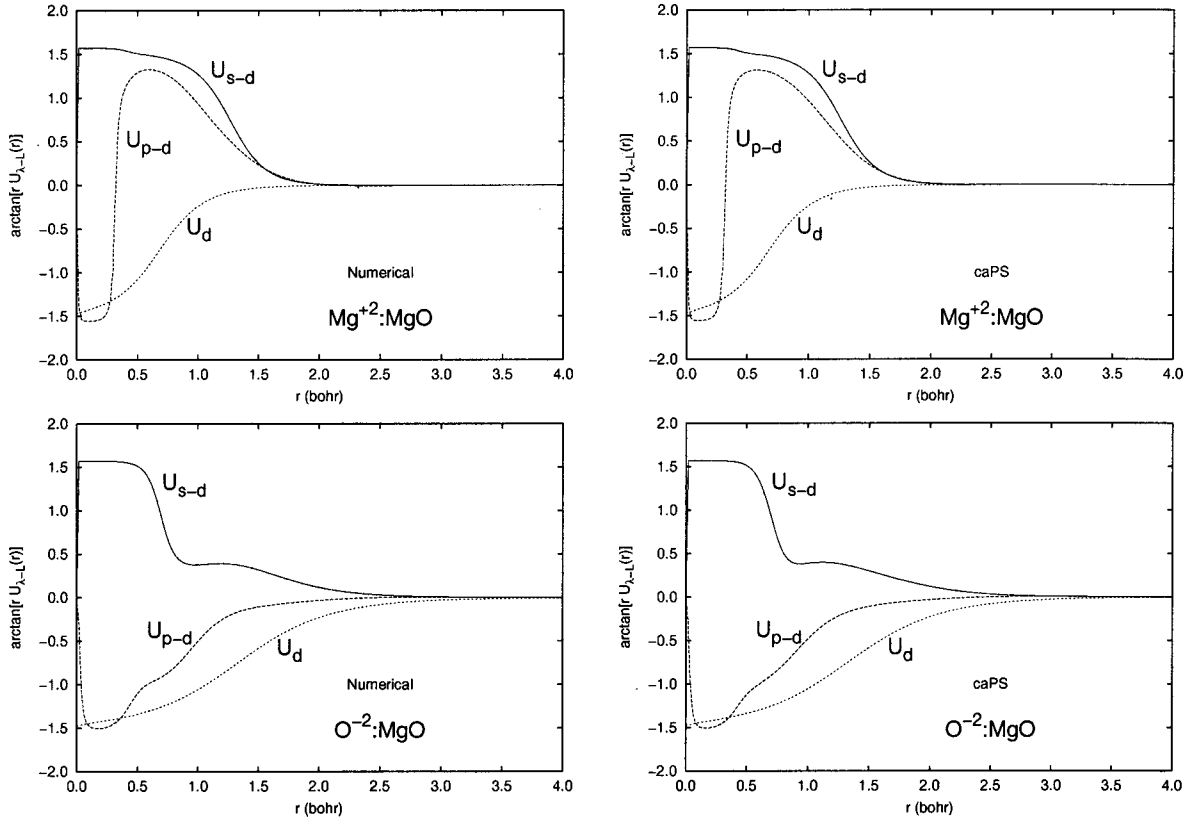


FIG. 1. Numerical (left) and fitted (right) CAPS for the $Mg^{2+}$ (up) and $O^{2-}$ (down) ions in MgO. Notice that the $\mathcal{U}_l(r)$ functions have very large positive and negative values. To improve the plot we use $\arctan[r\mathcal{U}_l(\nabla)]$ instead of $\mathcal{U}_l(r)$ because (a) the arctan( ) transformation maps the $(-\infty,+\infty)$ interval to $[-\pi/2,+\pi/2]$; (b) it preserves the sign of the argument; and (c) the small $|\mathcal{U}|$ region is undistorted, since $\lim_{y\to 0} y^{-1}\arctan y=1$.

sented in the fitting. To this end, the set of weights, $\{\sigma_k\}$, becomes important. The simplest model assigns equal weights to all grid points, $\sigma_k=1$. By using a weight proportional to the value of the function, $\sigma_k \propto |\mathcal{U}(r_k)|$, we can try to get a uniform relative error for all grid points.

## III. CRYSTAL ADAPTED PSEUDOPOTENTIALS FOR THE MgO CRYSTAL

Let us proceed now to determine crystal adapted pseudopotentials for the MgO crystal and test their behavior on the simulation of a number of neutral and charged defects. As a first step, we have done AIPI calculations[25,26] at the experimental geometry of the MgO crystal (lattice parameter $a=4.213$ Å), using the largest Slater-type Orbital (STO) basis sets proposed by Clementi and Roetti[38] for $O^-$ and $Mg^{2+}$. These calculations produce the orbital functions and energies for the ions in the crystal. It has been previously shown that the AIPI calculations predict the equilibrium properties and the equation of state of MgO in excellent agreement with the available experimental information.[39]

The second step corresponds to the numerical evaluation of the $\mathcal{U}_l(r)$ functions [Eqs. (19)–(21)] using the AIPI wave functions of MgO. Our results have been plotted in Fig. 1. We can observe that the qualitative aspects of the CAPS's are very similar in both ions. The $\mathcal{U}_l(r)$ functions have very large values near the nuclei, particularly for $l=s-L$. For instance, the $\mathcal{U}_{s-d}(r)$ function for $Mg^{2+}$ is $\approx 7.7\times 10^3$ at $r=0.06$ bohr. As the angular quantum number $l$ increases, the radial CAPS functions become less abrupt. All $\mathcal{U}_l(r)$ functions show a kind of shell structure, except the function that corresponds to the highest angular number, $\mathcal{U}_L(r)$, which is a negative and monotonically increasing function. All $\mathcal{U}_l(r)$ functions, on the other hand, approach zero as the distance from the nucleus increases. The *d* component becomes dominant at large distances.

We have found that 10–15 GTF's by symmetry, with exponents forming a geometrical series to prevent linear dependencies, allows an excellent and burden-free fitting of the numerical functions. However, such a large expansion would add impractically to the computational expense of a cluster-in-the-lattice calculation. Taking into account the normal limitations of the available molecular codes, 4–5 GTF's per radial function appears as a practical limit.

Under such circumstances, the CAPS fitting becomes a delicate problem. Accurate and useful fits require careful trying of the different optimization techniques and initial values of the parameters. The CAPS's contained in Table I constitute a compromise between a good fitting and a short expansion of the numerical AIPI embedding potentials. We have used 5 Gaussians per symmetry to provide an accuracy better than 6% at any point within the 0–3 bohr range. Figure 1 shows that the fitting is reasonable but not perfect.

TABLE I. $Mg^{2+}$ and $O^{2-}$ CAPS obtained from the AIPI calculation at the experimental geometry ($a=4.213$ Å) of MgO.

| $Mg^{2+}$ | $n_i$ | $B_i$ | $\alpha_i$ |
|---|---|---|---|
| $s-d$ | 2 | 202 752.811 410 000 | 259.834 541 790 |
| | 2 | 66 180.876 835 000 | 70.585 531 596 |
| | 2 | 5807.877 089 100 | 29.505 737 538 |
| | 2 | 51.817 572 229 | 3.225 356 163 |
| | 2 | 6.891 421 387 | 1.745 584 878 |
| $p$-$d$ | 2 | 1369.025 952 200 | 483.582 480 190 |
| | 2 | −1386.100 267 400 | 60.636 758 653 |
| | 2 | −29.960 840 154 | 7.327 324 917 |
| | 2 | 6.396 242 521 | 1.665 288 736 |
| | 3 | 62.197 933 908 | 5.627 393 157 |
| $d$ | 1 | −2.221 733 012 | 287.638 632 100 |
| | 1 | −2.205 452 222 | 26.153 807 145 |
| | 1 | −3.205 282 242 | 5.954 441 936 |
| | 1 | −1.754 934 219 | 2.421 788 124 |
| | 1 | −0.241 448 579 | 1.110 661 394 |
| $O^{2-}$ | $n_i$ | $B_i$ | $\alpha_i$ |
| $s$-$d$ | 2 | 179 14.022 901 000 | 66.130 524 945 |
| | 2 | 3656.939 912 700 | 21.194 327 172 |
| | 2 | 155.863 938 930 | 9.162 583 119 |
| | 2 | −3.975 007 998 | 3.589 159 280 |
| | 2 | 1.018 079 213 | 0.707 640 724 |
| $p$-$d$ | 2 | 157.952 553 650 | 189.985 416 720 |
| | 2 | −154.908 003 120 | 21.450 770 682 |
| | 2 | −6.435 733 717 | 2.870 414 868 |
| | 2 | −0.444 560 609 | 0.248 527 343 |
| | 3 | 0.253 338 453 | 0.306 313 051 |
| $d$ | 1 | −1.943 867 876 | 143.104 813 360 |
| | 1 | −1.888 123 352 | 12.807 469 812 |
| | 1 | −2.987 294 027 | 2.209 899 990 |
| | 1 | −2.523 696 496 | 0.763 464 773 |
| | 1 | −0.350 404 621 | 0.280 899 723 |

### Cluster model and self-embedding consistency

A first test on the previously derived CAPS's can be done by simulating the perfect MgO crystal using a cluster-in-the-lattice calculation. The ability to pass this self-embedding consistency test depends on (1) the cluster and lattice definition; (2) the basis set; and (3) the quantum technique used to determine the cluster wave function and energy.

The defect model is composed of a number of ions organized into three different regions. Obtaining the local wave function and energy of the cluster (region I) is the objective, so all the ions in this region add electrons and basis functions to the quantum-mechanical calculation. Region II is made of a collection of ions closely surrounding the cluster and represented by CAPS's. Region III, finally, comprises a number of point charges that simulate the Madelung field acting on the cluster volume. Our previous experience has shown us the convenience of dividing the cluster ions in subsets. Subset Ia is made of all ions that are geometrically and electronically relaxed in the calculation. Subset Ib contains the remaining cluster ions, whose positions are held fixed but their wave functions are allowed to relax.[40] The existence of the Ib region attenuates the effect of the cluster-lattice boundary on the cluster wave function.[40–42]

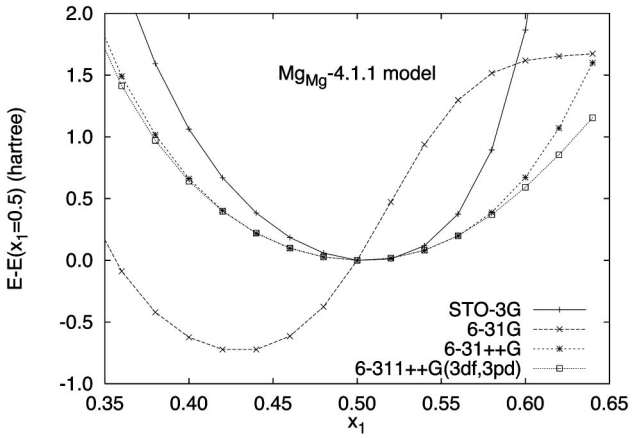


FIG. 2. Total energy of the $MgO_6^{10-}$ cluster versus the crystallographic position of the six O ligands, $x_1$. The calculations depicted on the plot are representative of the different types of behaviors found by using many different basis sets. The $Mg_{Mg}-4.1.1$ model was found to be self-embedding consistent when basis sets like 6-31++G or larger were used, the role of the diffuse functions on the O centers being essential for the consistency.

All the defects examined in this work are centered either on a Mg or an O position of the perfect lattice. It is then natural to organize its neighbors into shells of symmetrically equivalent ions around the substituted position. Accordingly, we will use the notation $A_B^z$–$m.n.p$ to designate the defect (following the common Kröger-Vink notation[43,44]) and the cluster model, where $m$ is the number of shells in regions I and II, $n$ the number of shells in region I, and $p$ the number of shells forming region Ia.

The simplest defect center model explored is $Mg_{Mg}-4.1.1$, in which a $MgO_6^{10-}$ quantum cluster is embedded by three shells of CAPS's [6 Mg at (1,0,0), 12 Mg at $(\frac{1}{2},\frac{1}{2},0)$, and 8 O at $(\frac{1}{2},\frac{1}{2},\frac{1}{2})$], plus a set of 336+6 point charges that will be presented later in some detail. We have done Hartree-Fock calculations using several different basis sets and the most interesting results have been represented in Fig. 2.

We can observe that the quality of basis sets associated with the cluster ions has significant effects on the nearest-neighbor equilibrium geometry. The use of minimal or small basis sets, such as STO-3G or 3-21G,[4] produces an equilibrium position that is reasonably close to the ideal $x_1=0.5$ value, but the nuclear potential is very asymmetric as it raises quite steeply for $x_1>0.5$. The use of large basis sets, which may include polarization functions but lack diffuse functions on the O centers, gives rise to absurd results, showing an optimal $x_1\approx 0.42$ and an unphysical lowering of the energy for $x_1\geqslant 0.55$. Physically sound results are recovered by including diffuse functions on the anions, and the use of any of 6-31++G, 6-311++G, 6-31++G($d$,$p$) or 6-311++G($d$,$p$) basis sets, for instance, produces almost identical results.

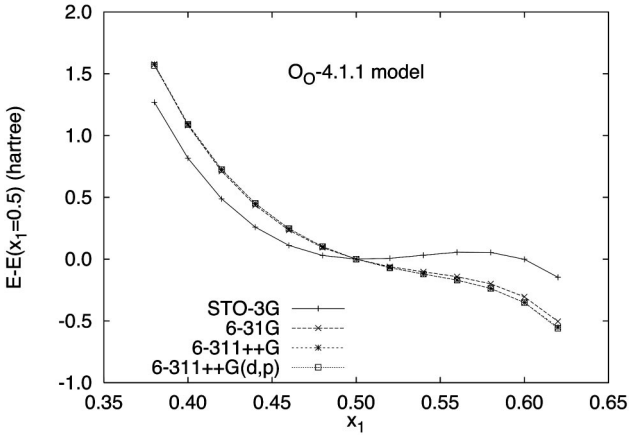


FIG. 3. Total energy of the $OMg_6^{10+}$ cluster versus the crystallographic position of the six Mg ligands, $x_1$, for the $O_O-4.1.1$ model. It is observed that the Mg ions collapse over the lattice with independence of the quality of the basis set used in the calculation.

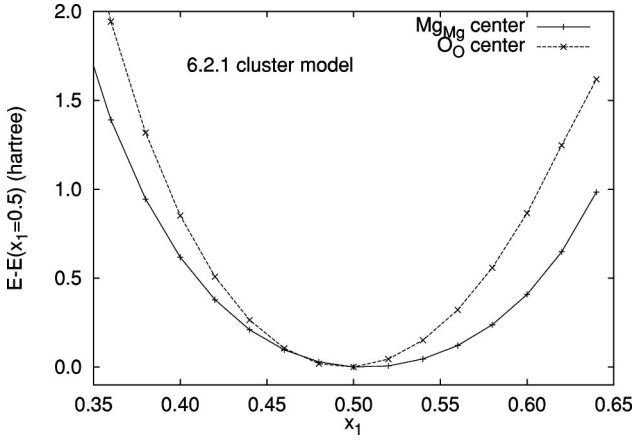


FIG. 4. Total energy of the $MgO_6Mg_6^{2+}$ and $OMg_6O_6^{2-}$ clusters versus the crystallographic position of the first shell of ligands, $x_1$. A 6-31G basis set has been used for $Mg^{2+}$ and 6-31++G for $O^{-2}$ ions.

A similar test can be done for the O-centered clusters. Figure 3 depicts the nuclear potential for the $OMg_6^{10+}$ cluster as obtained in the $O_O-4.1.1$ model calculations. It can be observed that the Mg shell collapses onto the lattice region no matter the quality of the basis set used in the calculation. This result must be seen as a serious limitation of the cluster model. We have previously discussed about the convenience of using cluster models in which the outmost shell, at least, of the quantum region is held fixed in position but otherwise allowed to relax electronically to respond to the changes in geometry of the inner quantum region.[40–42] The collapse observed on the $OMg_6^{10+}$ cluster appears as an extreme case of the inconsistency of small clusters discussed in Ref. 40.

The simplest models in which we can relax the position of the first shell of neighbors and still maintain a buffering shell within the cluster are $M_{\mathrm{Mg}}-6.2.1$ and $X_{\mathrm{O}}-6.2.1$. These contain 13 ions in the quantum region [the central ion, six neighbors at $(\frac{1}{2},0,0)$, and six neighbors at $(1,0,0)$], 32 ions represented by CAPS's [12 at $(\frac{1}{2},\frac{1}{2},0)$, 8 at $(\frac{1}{2},\frac{1}{2},\frac{1}{2})$, 6 at $(\frac{3}{2},0,0)$, and 6 at $(2,0,0)$] plus the set of point charges.

Figure 4 shows that all pathologies found previously on the 4.1.1 models have now been corrected. Both the $Mg^{2+}$-centered and the $O^{2-}$-centered clusters exhibit an equilibrium geometry for the first shell of neighbors that is very close to $x_1=0.5$, and a rather symmetric nuclear potential around the minimum. The 6.2.1 cluster model satisfies the self-embedding consistency test, and will be used in the next section to simulate a large number of MgO defect centers.

Before leaving this section we want to give some consideration to the representation of the Madelung field. It is well known that the electrostatic potential acting on a cluster electron constitutes a conditionally convergent series that must be added up using special techniques (see, for instance, Appendix B in Ref. 45). These techniques are, however, not available in most quantum mechanical molecular codes. Fortunately, Winter *et al.*[1,2] have shown that, at least for some crystal structures, the shape of the Madelung field in the cluster region can be reproduced by a finite set of point charges occupying their nominal positions and having their nominal charges. The actual value of the potential, much more difficult to converge, can be corrected by adding a small number of ghost ions situated far away from the cluster, with appropriately adjusted charges. The importance of accurately reproducing the electrostatic potential in all directions, not just along some particular axes, should be stressed as it can significantly influence the cluster electron density at the boundaries and the relative stability of the different orbital levels.

In the case of the rocksalt structure, the following set of point charges converges both to the shape and to the value of the Madelung field in the cluster region: (a) all lattice ions with crystal coordinates $-X_M \leqslant x,y,z \leqslant X_M$ and a nominal charge $q^S$; plus (b) six ghost charges at the $(\pm X_g,0,0)$ and equivalent positions by symmetry, with a charge $q^g$ adjusted to reproduce the exact Madelung potential at the cluster center. We have used in this work $X_M=3/2$ and $X_g=25$. This corresponds to a set of 342+6 point charges and reproduces the exact Madelung field to an error less than $4\times10^{-7}$ hartree at random points inside a sphere centered at the $(0,0,0)$ position with radius equal to the unit cell length $a$.

A limitation of the current molecular codes when performing cluster-in-the-lattice calculations, albeit small, deserves some comment. By default, the total energy computed for the cluster contains the self-energy of the embedding point charges. This has to be removed to get the effective energy of the cluster, i.e., the expectation value of the effective Hamiltonian [Eq. (1)]. Unphysical results would be obtained otherwise were cluster energies for different host geometries compared.

## IV. DEFECT CENTERS IN MgO

The final test on the usefulness of the embedding technique developed here is the examination of a large number of cationic and anionic defect centers: $M_{\mathrm{Mg}}$ and $X_{\mathrm{O}}$, respectively. We have used the 6.2.1 model described previously.

TABLE II. Results of the HF calculations on the $M^z_{Mg}-6.2.1$ cluster model of several cationic defects in MgO. The units used are hartrees for the cluster effective energy ($E^{opt}$); eV for the relaxation and formation energies; Å for the the NN displacement $\Delta R$; and $cm^{-1}$ for the $a_{1g}$ NN breathing mode frequency.

| Center | $M$ basis | $x_1^{opt}$ | $E^{opt}$ | $\Delta R_{relax}$ | $\Delta E_{relax}$ | | | $\omega_{a1g}$ |
|---|---|---|---|---|---|---|---|---|
| $Mg^{\times}_{Mg}$ | 6-31G | 0.507 206 | −1852.107 475 | +0.030 | −0.060 | | | 607 |
| Center | $M$ basis | $x_1^{opt}$ | $E^{opt}$ | $\Delta R$ | $\Delta E_{relax}$ | $\Delta E_f^{I}$ | $\Delta E_f^{II}$ | $\omega_{a1g}$ |
| $B^{\bullet}_{Mg}$ | 6-31G | 0.455 679 | −1676.757 596 | −0.217 | −1.670 | −40.221 | 7.460 | 559 |
| $Al^{\bullet}_{Mg}$ | 6-31G | 0.472 252 | −1894.310 298 | −0.147 | −0.901 | −28.199 | 1.528 | 638 |
| $Be^{\times}_{Mg}$ | 6-31G | 0.497 565 | −1667.066 241 | −0.041 | −0.006 | −4.374 | 0.348 | 551 |
| $Ca^{\times}_{Mg}$ | TZV | 0.525 984 | −2329.124 307 | +0.079 | −1.085 | 8.227 | 3.325 | 700 |
| $Ca^{\times}_{Mg}$ | Lan2DZ | 0.528 261 | −1688.649 543 | +0.089 | −1.271 | 6.982 | 2.087 | 702 |
| $Sr^{\times}_{Mg}$ | Lan2DZ | 0.538 698 | −1682.376 908 | +0.133 | −2.826 | 12.542 | 6.382 | 758 |
| $Ba^{\times}_{Mg}$ | Lan2DZ | 0.553 072 | −1676.957 612 | +0.193 | −6.734 | 19.767 | 12.087 | 855 |
| $Zn^{\times}_{Mg}$ | 6-311G | 0.510 893 | −3430.093 134 | +0.016 | −0.156 | −0.004 | 2.544 | 644 |
| $Li'_{Mg}$ | 6-31G | 0.534 923 | −1659.848 798 | +0.117 | −1.388 | 18.571 | 2.577 | 621 |
| $Na'_{Mg}$ | 6-31G | 0.541 548 | −1814.223 206 | +0.145 | −2.191 | 19.915 | 3.550 | 656 |
| $v''_{Mg}$ | — | 0.559 967 | −1652.044 909 | +0.222 | −4.645 | 24.038 | 12.717 | 707 |
| $v''_{Mg}$ | Mg:6-31G | 0.559 497 | −1652.061 303 | +0.220 | −4.266 | 33.592 | 12.271 | 684 |

The equilibrium geometry of the first shell of neighbors has been determined by performing single point calculations on a grid of 16 different geometries with $x_1$ going from 0.34 to 0.64. This totally symmetrical breathing ($a_{1g}$) movement of the nearest neighbors (NN's) has been the only geometry relaxation allowed in our calculations. The restricted Hartree-Fock (RHF) method has been used on the closed-shell clusters and the unrestricted Hartree-Fock (UHF) method on the open-shell ones. All calculations have been done with the GAUSSIAN94[3] and GAMESS[4] codes, using very strict convergence criteria. Particular care has been paid to secure that all calculations on a center converged to the same electronic state. Correlation energy has been shown to play ''no crucial role'' on the equilibrium properties of bulk and surface $F$ centers[46,47] and we expect the same behavior for the other defects examined here.

The main results are presented in Tables II and III. The 6-31G and 6-31++G basis sets have been used for the Mg and O atoms, respectively. The bases used for the other atoms in the impurity centers are collected in the tables. The equilibrium geometry ($x_1^{opt}$) and energy ($E^{opt}$) and the vibration frequency ($\omega_{a_{1g}}$) for the breathing movement of the NN's have been carefully determined by Marquardt-Levenberg least squares fitting of a high-degree polynomial to the cluster effective energy.

Our results show an outwards NN relaxation of +0.030 Å in $Mg_{Mg}$ and an inwards relaxation of −0.006 Å in $O_O$, which correspond to relaxation energies of −0.060 and −0.005 eV, respectively. This is a good degree of self-consistency, according to our experience.

Our predictions of the NN relaxation at the defect centers have been corrected for this small error in the calculation of the host. Accordingly, the NN displacement at a cationic defect is determined as

$$\Delta R = a(x_1^{opt} - x_1^{opt}[Mg^{\times}_{Mg}]), \tag{26}$$

and similarly for an anionic defect.

On the other hand, several definitions have been used in the literature for the formation energy of the defect. The two main conventions use either ions or neutral atoms, respectively, according to the formal chemical reactions:

$$\text{(I)} \quad Mg^{2+}{:}MgO_{(s)} + A^{2+}_{(g)} \rightarrow A^{2+}{:}MgO_{(s)} + Mg^{2+}_{(g)}$$

and

$$\text{(II)} \quad Mg^{2+}{:}MgO_{(s)} + A_{(g)} \rightarrow A^{2+}{:}MgO_{(s)} + Mg_{(g)}$$

for the cationic defects, and similarly for the anionic ones. Very large differences are found between the formation energies in both conventions: $\Delta E_f^{I}$ and $\Delta E_f^{II}$, respectively. In addition, the Gaussian basis sets routinely used for the molecular calculations are rather far away from the Hartree-Fock limit for free atoms and anions, which adds significantly to the errors in the formation energies. Particularly difficult is obtaining a physically significant reference energy for $O^{2-}$ and $S^{2-}$ because of their instability as free, gas-phase entities. To avoid these problems when comparing our results to those by other researchers, we list both types of formation energies in Tables II and III.

Let us now examine the most significant aspects of our predictions. We can observe that the defects can be naturally grouped by their type (cationic or anionic) and charge. As a general rule, cationic defects tend to produce large inwards displacements when charged positively, small relaxations if neutral, and outwards displacements when charged negatively. The opposite is true for the anionic defects. This trend is in agreement with the sign of the Madelung field at the $Mg^{2+}$ and $O^{2-}$ host positions, revealing that the phenomenon is largely influenced by the electrostatic interactions.

TABLE III. Results of the HF calculations on the $X_O^z - 6.2.1$ cluster model of several anionic defects in MgO. The units used are the same as in Table II.

| Center | $M$ basis | $x_1^{opt}$ | $E^{opt}$ | $\Delta R_{relax}$ | $\Delta E_{relax}$ | | | $\omega_{a1g}$ |
|---|---|---|---|---|---|---|---|---|
| $O_O^\times$ | 6-31++G | 0.498 532 | −1728.871 865 | −0.006 | −0.005 | | | 678 |
| Center | $A$ basis | $x_1^{opt}$ | $E^{opt}$ | $\Delta R$ | $\Delta E_{relax}$ | $\Delta E_f^I$ | $\Delta E_f^{II}$ | $\omega_{a1g}$ |
| $H_O^{\bullet\bullet}$ ($H^0$) | 6-31++G | 0.550 052 | −1653.644 129 | +0.217 | −1.492 | 35.801 | 25.784 | 458 |
| $v_O^{\bullet\bullet}$ ($F^{+2}$) | — | 0.547 710 | −1653.181 805 | +0.207 | −6.126 | 34.809 | 24.791 | 784 |
| $v_O^{\bullet\bullet}$ ($F^{+2}$) | H:6-31++G | 0.548 006 | −1653.191 811 | +0.208 | −5.667 | 34.537 | 24.519 | 763 |
| $v_O^{\bullet\bullet}$ ($F^{+2}$) | O:6-31++G | 0.547 801 | −1653.184 417 | +0.208 | −5.718 | 34.738 | 24.720 | 766 |
| $H_O^{\bullet}$ ($H^-$) | 6-31++G | 0.523 563 | −1654.239 927 | +0.105 | −1.216 | 19.269 | 9.571 | 681 |
| $F^+$ | — | 0.526 777 | −1653.545 595 | +0.119 | −1.656 | 24.909 | 14.892 | 701 |
| $F^+$ | H:6-31++G | 0.520 839 | −1653.615 439 | +0.094 | −1.196 | 16.693 | 12.991 | 768 |
| $F^+$ | O:6-31++G | 0.523 693 | −1653.457 947 | +0.106 | −1.219 | 24.277 | 17.277 | 666 |
| $F_O^{\bullet}$ | 6-31++G | 0.522 254 | −1753.246 715 | +0.100 | −1.112 | 17.188 | 5.814 | 686 |
| $Cl_O^{\bullet}$ | 6-31++G(d) | 0.535 466 | −2113.253 617 | +0.156 | −3.407 | 21.029 | 8.530 | 747 |
| $Br_O^{\bullet}$ | 6-311++G(d) | 0.539 993 | −4227.026 553 | +0.175 | −4.600 | 23.642 | 11.145 | 766 |
| $S_O^\times$ | 6-31++G(d) | 0.520 716 | −2051.445 510 | +0.093 | −1.193 | 8.795 | 3.217 | 756 |
| $Se_O^\times$ | 6-311++G(d) | 0.527 520 | −4053.622 241 | +0.122 | −2.162 | 13.133 | 6.954 | 761 |
| $F$ | — | 0.507 619 | −1653.678 726 | +0.038 | −0.068 | 21.287 | 11.269 | 489 |
| $F$ | H:6-31++G | 0.498 570 | −1653.766 094 | 0.000 | −0.003 | −5.343 | 8.892 | 597 |
| $F$ | O:6-31++G | 0.500 991 | −1653.759 796 | +0.010 | −0.002 | 5.418 | 9.063 | 585 |
| $N_O'$ | 6-31++G(d) | 0.481 536 | −1708.317 033 | −0.072 | −0.730 | −11.141 | 4.411 | 688 |
| $P_O'$ | 6-31++G(d) | 0.512 497 | −1994.419 305 | +0.059 | −0.413 | 4.356 | 9.877 | 729 |
| $As_O'$ | 6-311++G(d) | 0.517 564 | −3887.780 659 | +0.080 | −0.746 | 8.768 | 12.660 | 689 |

$M_{Mg}^{\bullet}$ *centers*. $B^{3+}$ and $Al^{3+}$ are considerably smaller than $Mg^{2+}$ and induce significant inwards NN relaxations: $-0.22$ and $-0.15$ Å, respectively. Both centers are unstable according to criterion II, but the formation energies are very large and negative according to criterion I. The value $\Delta E_f^I(Al_{Mg}^{\bullet}) = -28.2$ eV can be compared with the estimation of Colbourn and Mackrodt[48] using the shell model and Gordon-Kim type potentials: $-30.29$ eV.

Our cluster calculations do not take into account the long range polarization energy associated to the formation of a charged defect. Using a simple dielectric continuum model, the polarization energy around a cavity of radius $R$ is given by[49]

$$E_{pol} = \frac{Q^2}{2R}(1 - 1/\epsilon_0), \tag{27}$$

where $Q$ is the net charge of the defect and $\epsilon_0$ the static dielectric constant of MgO. Using $R = a\sqrt{5}/2$ (the position of the first neighbor shell beyond the cluster) we estimate $E_{pol}$ to be $\approx 1$ eV for the $Q = \pm 1$, and $\approx 4$ eV for the $Q = \pm 2$ defects. Going beyond this crude but widely used model[49–54] can be done by calculating neutral associations of defects and obtaining a statistical average over the many different charge compensation mechanisms[55] but this is well beyond the current possibilities of present *ab initio* calculations.

$M_{Mg}^{\times}$ *centers*. The replacement of $Mg^{2+}$ by another divalent closed-shell ion produces a very simple result, easy to interpret in terms of the relative ionic radii of $M^{2+}$ and $Mg^{2+}$. Accordingly, the NN shell relaxes inwards when $M$ = Be and outwards for the other alkaline-earth metals and Zn. The actual value of the relaxation is, however, significantly smaller than the difference in the generally accepted ionic radii:[56] 0.45 ($Be^{2+}$), 0.720 ($Mg^{2+}$), 1.00 ($Ca^{2+}$), 1.18 ($Sr^{2+}$), 1.35 ($Ba^{+2}$), and 0.740 ($Zn^{+2}$). The net effect of the MgO lattice is then to damp the differences in size among the alkaline-earth-metal cations. The formation energy of all $M_{Mg}^{\times}$ centers is positive, according to criterion II, and increases as the difference in size between $M^{2+}$ and $Mg^{2+}$ increases. If criterion I is used, instead, the formation energies are lowered by 2–7 eV and, in fact, $Be_{Mg}^{\times}$ becomes stable. Our values of $\Delta E_f^I$ for $Be_{Mg}^{\times}$ ($-4.37$ eV) and $Ca_{Mg}^{\times}$ ($+8.23$ eV) are in reasonable agreement with the shell-model calculations by Colbourn and Mackrodt:[48] $-3.57$ and $+5.82$ eV, respectively.

The breathing mode vibration frequency, on the other hand, increases with the size of the $M^{2+}$ ion. This is not a mass effect, as the effective mass of the $1a_{1g}$ mode, $6m_O$, is independent of $M^{2+}$, but a direct consequence of the increasing force constant as $M^{2+}$ becomes larger.

It is worth mentioning that the calculations on the heavy ions $Sr^{2+}$ and $Ba^{2+}$ have been done using Hay and Wadt relativistic ECP's to represent the core electrons,[57,13,58] because Gaussian all-electron basis sets of quality are not available. Test calculations on the $Ca_{Mg}^{\times}$ center show that the valence-electron calculations agree with the all-electron results within 0.01 Å on the center geometry and within 2

$cm^{-1}$ on the nuclear potential curvature. This agreement evidences the usefulness of the valence-electron calculations on the heavy elements.

*$M'_{Mg}$ centers*. The net charge of the defect, $-1$, dominates the center geometry and both $Li'_{Mg}$ and $Na'_{Mg}$ induce a significant outwards relaxation: $+0.12$ and $+0.15$ Å, respectively, very similar to the values reported by Grimes *et al.*[49] The formation energy of both centers is very similar: 3–4 eV using criterion II and 19–20 eV using criterion I. The last value can be compared to the shell-model classical estimation of 16.3 ($Li'_{Mg}$) and 18.6 eV ($Na'_{Mg}$).[48]

*$Mg^{2+}$ vacancy ($v''_{Mg}$) center*. This highly charged defect induces a very large outwards relaxation on the NN shell: $+0.22$ Å. We could also expect a noticeable relaxation of even further shells of neighbors, which has not been taken into account in our calculations. In consequence, our calculated formation energy, $\approx 34$ eV (criterion I) should be considered as an upper limit value. As a comparison, the shell-model classical calculations by Colbourn and Mackrodt[48] produce $\Delta E_f^{\mathrm{I}} = +25.41$ eV after allowing for the relaxation of many shells around the defect center. Gibson *et al.*, on the other hand, predict $\Delta E_f^{\mathrm{II}} = +13.82$ eV,[59] close to our value of $+12.27$ eV.

We have examined the effect of the basis set on the vacancy center by doing the calculation, both maintaining the $Mg^{2+}$ basis at the vacancy position and removing it. Both calculations show a negligible difference in the center geometry, but the use of basis functions at the vacancy position reduces the total energy of the cluster by some 0.5 eV and the $1a_{1g}$ breathing frequency by 23 $cm^{-1}$.

*$X^{\bullet}_{O}$ centers*. The positive charge of the defect produces a significant outwards relaxation ($+0.10$ Å for $F^{\bullet}_{O}$), which is further enhanced if the ionic radius of the impurity anion is larger than that of the oxide. The relaxations are, however, quite different from the differences in ionic radii:[56] 1.19 ($F^-$), 1.26 ($O^{-2}$), 1.67 ($Cl^-$), and 1.82 Å ($Br^-$). We see, again, that the lattice damps the difference in size between the substitute and the host ions. On the other hand, our value for $\Delta E_f^{\mathrm{I}}(F^{\bullet}_{O}) = +17.19$ eV agrees with the shell-model estimation reported by Catlow:[60] $+16.31$ eV. The center stability decreases in passing from F to Cl and Br, and the nuclear potential curvature, as measured by $\omega_{a1g}$, increases along the same series.

*$X^{\times}_{O}$ centers*. Our calculations predict outwards relaxations for both $S^{\times}_{O}$ and $Se^{\times}_{O}$ centers, but much smaller than the ionic radii difference (1.40, 1.80, and 1.98 Å for $O^{2-}$, $S^{2-}$, and $Se^{2-}$, respectively[56]). Our results, $+4.4\%$ and $+5.8\%$, are more in line with the previous ICECAP calculations by Pandey *et al.*:[61] $\sim 6\%$ and $\sim 8\%$ outwards NN displacements for $S^{\times}_{O}$ and $Se^{\times}_{O}$, respectively.

*$X'_{O}$ centers*. The $N'_{O}$ center shows the tendency of negative anionic defects to suffer small inwards NN relaxations. In the case of the $P'_{O}$ and $As'_{O}$ centers, the bigger size of the third- and fourth-period anions works against this tendency to produce a small outwards NN displacement.

The results on the N–As, O–Se, and F–Br groups of impurities show that for a given group the difference between the third- and fourth-period ions is significantly smaller than that between the second- and third-period ions. In other words, the head of group elements (N, O, F) behave differently from the other elements in their group. This well-known effect for pure crystals and gas phase molecules appears again in substitutional impurities.

*$F$ centers [$F \equiv (v^{\bullet\bullet}_{O} + 2e')^{\times}$, $F^+ \equiv (v^{\bullet\bullet}_{O} + e')^{\bullet}$, $F^{+2} \equiv v^{\bullet\bullet}_{O}$]:* Our calculations predict a negligible distortion of the lattice for the neutral $F$ center, significant outwards NN relaxation for $F^+$ ($+0.09$ Å), and even larger outwards displacement for $F^{+2}$ ($+0.21$ Å). As in the case of the cationic vacancy, we have explored the effect of including or not basis set functions at the oxygen vacancy, i.e., using floating basis functions. The smallest cluster energy is obtained when a $H^-$ basis set is used on this position. The effect is small on the NN geometry (0.04 Å in the worst case: $F$ center with no basis) but it can be of several eV's on the formation energy of the $F$ and $F^+$ centers.

$F$ centers are the best investigated MgO defects, both from an experimental[62–68] and from a theoretical point of view (Refs. 46,47,49,50,53,54,59,69–76). Our results compare well with, for instance, the EMBED calculations by Scorza *et al.*[46] and the density-functional theory (DFT) 32-molecule supercell calculations by Kantorovich *et al.*[74] The local density approximation (LDA) 8-molecule supercell calculations by Wang and Holzwarth[71] differ, however, in predicting much smaller relaxations for the charged $F$ centers. Our $\Delta E_f^{\mathrm{II}}$ formation energies, on the other hand, do agree with the classical Mott-Littleton simulations[60,77] as well as with other quantum-mechanical calculations.[46,74]

## V. CONCLUSIONS

We have presented a method of deriving crystal adapted pseudopotentials for positive, neutral, or negative atomic species. Our CAPS's provide a practical solution to the embedding problem for cluster-in-the-lattice calculations, as they are immediately supported in many available molecular codes.

To test the accuracy and reliability of our technique, we have considered a well-known ionic compound, MgO. Either a $MgO_6Mg_6$ or $OMg_6O_6$ quantum cluster embedded in the CAPS plus a carefully chosen set of point charges has been used to determine the equilibrium properties of several cationic and anionic, neutral, and charged defect centers. Our results are overall consistent and do compare well with previous calculations using many different techniques. This comparison should not hide the fact that we have used a single method and cluster model, rather than a tailored scheme for each type of defect center. We believe that the CAPS can be a valuable resource for other researchers and we plan to derive and make publicly available the potentials for some of the most common ions and host lattices.

## ACKNOWLEDGMENTS

V.L. thanks the staff of the Physics Department of the

Michigan Technological University, Andrea Suomi in particular, for their help in providing a pleasant and fruitful environment. This work was initially supported by the NATO Collaborative Research Grants Program under Grant No. CRG-921348. Oviedo's team was supported by the Spanish Ministerio de Educación y Ciencia (Grant No. PB96-0559) and Ministerio de Ciencia y Tecnología (Grant No. BQU2000-0466).

[1] N. W. Winter, R. M. Pitzer, and D. K. Temple, J. Chem. Phys. **86**, 3549 (1987).
[2] N. W. Winter, R. M. Pitzer, and D. K. Temple, J. Chem. Phys. **87**, 2945 (1987).
[3] M. J. Frisch, G. W. Trucks, H. B. Schlegel, P. M. W. Gill, B. G. Johnson, M. A. Robb, J. R. Cheeseman, T. Keith, G. A. Petersson, J. A. Montgomery, K. Raghavachari, M. A. Al-Laham, V. G. Zakrzwoski, J. V. Ortiz, J. B. Foresman, J. Cioslowski, B. B. Stefanov, A. Nanayakkara, M. Challacombe, C. Y. Peng, P. Y. Ayala, W. Chen, M. W. Wong, J. L. Andres, E. S. Repogle, R. Gomperts, R. L. Martin, D. J. Fox, J. S. Binkley, D. J. Defrees, J. Baker, J. J. P. Stewart, M. Head-Gordon, C. Gonzalez, and J. Pople, *Gaussian94, Revision E.2* (Gaussian Inc., Pittsburgh, PA, 1995).
[4] M. W. Schmidt, K. K. Baldridge, J. A. Boatz, S. T. Elbert, M. S. Gordon, J. H. Jensen, S. Koseki, N. Matsunaga, K. A. Nguyen, S. J. Su, T. L. Windus, M. Dupuis, and J. A. Montgomery, J. Comput. Chem. **14**, 1347 (1993); web page: http://www.msg.ameslab.gov/GAMESS/GAMESS.html
[5] R. Shepard, I. Shavitt, R. M. Pitzer, D. C. Comeau, M. Pepper, H. Lischka, P. G. Szalay, R. Ahlrichs, F. B. Brown, and J.-G. Zhao, Int. J. Quantum Chem. **S22**, 149 (1988); see also the web page for the current versions: http://www.itc.univie.ac.at/~hans/Columbus/columbus.html
[6] M. Dupuis, A. Farazdel, S. P. Karna, and S. A. Maluendes, in *MOTECC'90: Modern Techniques in Computational Chemistry*, edited by E. Clementi (ESCOM Science Publishers, Leiden, The Netherlands, 1990), p. 277.
[7] J. M. Vail, R. Pandey, and A. B. Kunz, Rev. Solid State Sci. **5**, 241 (1991).
[8] Z. Barandiarán and L. Seijo, J. Chem. Phys. **89**, 5739 (1988).
[9] V. Luaña and L. Pueyo, Phys. Rev. B **39**, 11 093 (1989).
[10] C. Pisani, R. Orlando, and F. Corà, J. Chem. Phys. **97**, 4195 (1992).
[11] J. L. Pascual and L. Seijo, J. Chem. Phys. **102**, 5368 (1995).
[12] L. F. Pacios and P. A. Christiansen, J. Chem. Phys. **82**, 2664 (1985), also references therein.
[13] W. R. Wadt and P. J. Hay, J. Chem. Phys. **82**, 284 (1985), also references therein.
[14] T. R. Cundari and W. J. Stevens, J. Chem. Phys. **98**, 5555 (1993), also references therein.
[15] N. W. Winter, D. K. Temple, V. Luaña, and R. M. Pitzer, in *Advances in Molecular Electronic Structure Theory*, edited by T. H. Dunning (JAI Press, New York, 1994), Vol. 2, pp. 61–109.
[16] N. W. Winter and R. M. Pitzer, J. Chem. Phys. **89**, 446 (1988).
[17] N. W. Winter, M. Ross, and R. M. Pitzer, J. Phys. Chem. **94**, 1172 (1990).
[18] N. W. Winter and C. E. Violet, Physica C **162**, 261 (1989).
[19] R. L. Martin, in *Cluster Models for Surface and Bulk Phenomena*, edited by G. Pacchioni, P. Bagus, and F. Parmigiani (Plenum, New York, 1992), p. 485.
[20] R. L. Martin and P. J. Hay, J. Chem. Phys. **98**, 8680 (1993).
[21] N. W. Winter, C. I. Merzbacher, and C. E. Violet, Appl. Spectrosc. Rev. **28**, 123 (1993).
[22] R. L. Martin, Phys. Rev. Lett. **75**, 744 (1995).
[23] P. Hüsser, H. U. Suter, E. P. Stoll, and P. F. Meier, Phys. Rev. B **61**, 1567 (2000).
[24] S. Huzinaga, L. Seijo Z. Barandiarán, and M. Klobukowski, J. Chem. Phys. **86**, 2132 (1987).
[25] V. Luaña and L. Pueyo, Phys. Rev. B **41**, 3800 (1990).
[26] M. A. Blanco, V. Luaña, and A. Martín Pendás, Comput. Phys. Commun. **103**, 287 (1997).
[27] R. McWeeny and B. T. Sutcliffe, *Methods of Molecular Quantum Mechanics* (Academic, London, 1969).
[28] S. Huzinaga, D. McWilliams, and A. A. Cantú, Adv. Quantum Chem. **7**, 187 (1973).
[29] E. Francisco, A. Martín Pendás, and W. H. Adams, J. Chem. Phys. **97**, 6504 (1992).
[30] W. H. Adams, J. Chem. Phys. **34**, 89 (1961).
[31] W. H. Adams, J. Chem. Phys. **37**, 2009 (1962).
[32] T. L. Gilbert, in *Molecular Orbitals in Chemistry*, edited by P. O. Lowdin and B. Pullman (Academic, New York, 1964).
[33] A. B. Kunz, Phys. Status Solidi **36**, 301 (1969).
[34] A. Martín Pendás, E. Francisco, and J. M. Recio, J. Chem. Phys. **97**, 452 (1992).
[35] E. R. Davidson, in *MOTECC'90: Modern Techniques in Computational Chemistry*, edited by E. Clementi (ESCOM Science Publishers, Leiden, The Netherlands, 1990), p. 553.
[36] L. R. Kahn, P. Baybutt, and D. G. Truhlar, J. Chem. Phys. **65**, 3826 (1976).
[37] W. H. Press, B. P. Flannery, S. A. Teukolsky, and W. T. Vetterling, *Numerical Recipes* (Cambridge Univ. Press, Cambridge, 1986).
[38] E. Clementi and C. Roetti, At. Data Nucl. Data Tables **14**, 177 (1974).
[39] V. Luaña, J. M. Recio, and L. Pueyo, Phys. Rev. B **42**, 1791 (1990).
[40] V. Luaña and M. Flórez, J. Chem. Phys. **97**, 6544 (1992).
[41] V. Luaña, M. Flórez, and L. Pueyo, J. Chem. Phys. **99**, 7970 (1993).
[42] M. Flórez, M. A. Blanco, V. Luaña, and L. Pueyo, Phys. Rev. B **49**, 69 (1994).
[43] F. A. Kröger and H. H. Vink, in *Solid State Physics*, edited by F. Seitz and D. Turnbull (Academic, San Diego, 1956), pp. 307–435.
[44] F. A. Kröger, *The Chemistry of Imperfect Crystals* (North-Holland, Amsterdam, 1964).
[45] C. Kittel, *Introduction to Solid State Physics*, 7th ed. (Wiley, New York, 1996).
[46] E. Scorza, U. Birkenheuer, and C. Pisani, J. Chem. Phys. **107**, 9645 (1997).
[47] F. Illas and G. Pacchioni, J. Chem. Phys. **108**, 7835 (1998).
[48] E. A. Colbourn and W. C. Mackrodt, J. Mater. Sci. **17**, 3021 (1982).

[49] R. W. Grimes, C. R. A. Catlow, and A. M. Stoneham, J. Phys.: Condens. Matter **1**, 7367 (1989).
[50] J. M. Vail, A. H. Harker, J. H. Harding, and P. Saul, J. Phys. C **17**, 3401 (1984).
[51] A. D. Vita, M. J. Gillan, J. S. Lin, M. C. Payne, I. Štich, and L. J. Clarke, Phys. Rev. B **46**, 12 964 (1992).
[52] M. J. Gillan, I. Manassidis, and A. D. Vita, Philos. Mag. B **69**, 879 (1994).
[53] C. Pisani, F. Corà, R. Dovesi, and R. Orlando, J. Electron Spectrosc. Relat. Phenom. **69**, 1 (1994).
[54] A. M. Ferrari and G. Pacchioni, J. Phys. Chem. **99**, 17 010 (1995).
[55] W. H. Gourdin and W. D. Kingery, J. Mater. Sci. **14**, 2053 (1979).
[56] R. D. Shannon, Acta Crystallogr., Sect. A: Cryst. Phys., Diffr., Theor. Gen. Crystallogr. **32**, 751 (1976).
[57] P. J. Hay and W. R. Wadt, J. Chem. Phys. **82**, 270 (1985).
[58] P. J. Hay and W. R. Wadt, J. Chem. Phys. **82**, 299 (1985).
[59] A. Gibson, R. Haydock, and J. P. LaFemina, Phys. Rev. B **50**, 2582 (1994).
[60] C. R. A. Catlow, Cryst. Lattice Defects Amorphous Mater. **14**, 223 (1987).
[61] R. Pandey, J. Zuo, and A. B. Kunz, Phys. Rev. B **39**, 12 565 (1989).
[62] W. P. Unruh and J. W. Culvahouse, Phys. Rev. **154**, 861 (1967).
[63] L. A. Kappers, R. L. Kroes, and E. Hensley, Phys. Rev. B **1**, 4151 (1970).
[64] A. J. Tench and M. J. Duck, J. Phys. C **6**, 1134 (1973).
[65] Y. Chen, R. Gonzalez, and O. E. Schow, and G. P. Summers, Phys. Rev. B **27**, 1276 (1983).
[66] G. P. Summers, T. M. Wilson, B. T. Jeffries, H. T. Tohver, Y. Chen, and M. M. Abraham, Phys. Rev. B **27**, 1283 (1983).
[67] J. Tombrello, H. T. Tohver, Y. Chen, and T. M. Wilson, Phys. Rev. B **30**, 7374 (1984).
[68] G. H. Rosenblat, M. W. Rowe, G. P. W. Jr., R. T. Williams, and Y. Chen, Phys. Rev. B **39**, 10 309 (1989).
[69] D. E. Taurian, A. H. Tang-Kai, and V. Lobatch, J. Phys. Chem. Solids **47**, 59 (1986).
[70] B. M. Klein, W. E. Pickett, L. L. Boyer, and R. Zeller, Phys. Rev. B **35**, 5802 (1987).
[71] Q. S. Wang and N. A. W. Holzwarth, Phys. Rev. B **41**, 3211 (1990).
[72] J. M. Vail, J. Phys. Chem. Solids **51**, 589 (1990).
[73] K. Jackson, M. R. Pederson, and B. M. Klein, Phys. Rev. B **43**, 2364 (1991).
[74] L. N. Kantorovich, J. M. Holender, and M. J. Gillan, Surf. Sci. **343**, 221 (1995).
[75] R. A. Evarestov, P. W. M. Jacobs, and A. V. Leko, Phys. Rev. B **54**, 8969 (1996).
[76] G. Pacchioni, A. M. Ferrari, and G. Ieranò, Faraday Discuss. **106**, 155 (1997).
[77] R. W. Grimes and C. R. A. Catlow J. Am. Ceram. Soc. **73**, 3251 (1990).